International Journal of Biological Macromolecules 265 (2024) 130793

Contents lists available at ScienceDirect

International Journal of Biological Macromolecules

journal homepage: www.elsevier.com/locate/ijbiomac

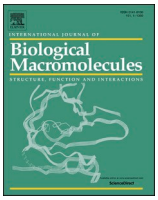

Polymerization strategy for cellulose nanocrystals-based photonic crystal films with water resisting property

Yue Zhang, De-qiang Li *, Cai-xia Yang, Zi-wei Xiong, Maryamgul Tohti, Yu-qing Zhang, Hong-jie Chen, Jun Li *

College of Chemistry and Chemical Engineering, Xinjiang Agricultural University, Urumchi 830052, China

ARTICLE INFO

Keywords:
Cellulose nanocrystal
Polyacrylamide
Self-assembly
Chiral liquid crystal
Graft polymerization

ABSTRACT

Cellulose nanocrystals (CNCs) can form a liquid crystal film with a chiral nematic structure by evaporative-induced self-assembly (EISA). It has attracted much attention as a new class of photonic liquid crystal material because of its intrinsic, unique structural characteristics, and excellent optical properties. However, the CNCs-based photonic crystal films are generally prepared via the physical crosslinking strategy, which present water sensitivity. Here, we developed CNCs-*g*-PAM photonic crystal film by combining free radical polymerization and EISA. FT-IR, SEM, POM, XRD, TG-DTG, and UV–Vis techniques were employed to characterize the physicochemical properties and microstructure of the as-prepared films. The CNCs-*g*-PAM films showed a better thermo-stability than CNCs-based film. Also, the mechanical properties were significantly improved, viz., the elongation at break was 9.4 %, and tensile strength reached 18.5 Mpa, which was a much better enhancement than CNCs-based film. More importantly, the CNCs-*g*-PAM films can resist water dissolution for more than 24 h, which was impossible for the CNCs-based film. The present study provided a promising strategy to prepare CNCs-based photonic crystal film with high flexibility, water resistance, and optical properties for applications such as decoration, light management, and anti-counterfeiting.

1. Introduction

Chiral nematic materials have been the focus of research for a long time and have many potential applications, including anti-counterfeiting materials, wearable functional materials, and biomaterials. As early as 1949, Onsager declared that the nanomaterials with rigid-rod structures could have an orientational (or nematic) pattern via the repulsive forces. Recently, many feedstocks have been employed to form chiral nematic materials, such as tobacco mosaic virus, DNA fragments, flagella filaments, collagen, boehmite, chitin, and κ-carrageenan [1–3]. Cellulose nanocrystals (CNCs), cellulose-rich raw materials derived nanoparticles via acid hydrolysis, can also have the self-assembly ability to form orientational structure, as well as the advantages in mechanical strength and optical property compared with the abovementioned feedstocks [4].

Sulfuric acid is commonly used to obtain the CNCs that consequently possess sulfate hemiester groups on their surface; the surface negative charges and the helical structure of CNCs endowed the feasibility to form the orientational pattern [5–7]. More importantly, the chiral nematic structure still exists even after the slow evaporation of water, thus forming CNCs-based photonic films with left-handed circular helical structures [8–10]. However, the pure CNCs based film can not only show fragile but also soluble, limiting its functional application based on assembly characteristics [11,12]. To overcome this defect, easy-get polymers have been introduced in the CNCs-based photonic crystal films that showed improved flexibility and mechanical strength via noncovalent forces, such as polyvinyl alcohol (PVA) [13] and polyethylene glycol (PEG) [14–16]. The addition of the polymers can adjust the color of the film by changing the pitch size [13]. In addition, biomass materials have a wide range of applications, such as drug delivery [17,18] and textile surface modification [19]. However, this strategy is unquestionably ineffective under specific conditions due to the excellent hydrophilia of the components, such as that with high humidity or in aqueous solution.

Hydrophobic surface modification of CNCs can significantly decrease the solubility or wettability in aqueous solution [20]. Still, the as-prepared films were generally formed via noncovalent forces, and only in rare cases can high-performance membrane materials be obtained. Covalent crosslinking is an effective strategy for developing membrane

* Corresponding authors.
E-mail addresses: lsx20131120a@163.com, ldq@xjau.edu.cn (D.-q. Li), Junli107@163.com (J. Li).

https://doi.org/10.1016/j.ijbiomac.2024.130793
Received 24 November 2023; Received in revised form 26 February 2024; Accepted 9 March 2024
Available online 17 March 2024

materials in which the covalent linkage-induced shrinkage force can counteract the thermodynamic force of swelling in the aqueous solution. Thus, many works were performed via covalent crosslinking strategies such as Schiff base reaction and free radical polymerization [21]. Thereinto, CNCs were generally used as additives to enhance the mechanical properties of the as-prepared materials that missed the circular helical structures.

The objective of the present study is to study the feasibility of a combination of free radical polymerization and evaporation-induced self-assembly (EISA) to form a CNCs-based photonic crystal film. Here, acrylamide was collected as the representative of vinyl monomers, and the obtained polyacrylamide (PAM) component may enhance the mechanical properties (i.e., elongation at break and tensile modulus). The obtained CNCs-*g*-PAM hybrid films were characterized by FT-IR, XRD, TG-DTG, SEM, POM, and UV–vis techniques. Moreover, their mechanical properties were also determined. Results showed that the combination of polymerization and EISA is an effective strategy for forming CNCs-based photonic crystal films. Compared with the pure CNCs-based photonic crystal films, the as-prepared films presented significant improvements in mechanical properties and solvent resistance. This strategy can be extended to other free radical polymerizations.

2. Materials and methods

2.1. Materials

CNCs were self-prepared via the typical H_2SO_4 hydrolysis of long-staple cotton that was obtained from a local farm in Shihezi, China. Sulfuric acid (H_2SO_4, 98 wt%), PVA, PEG (Mw = 9000–12,000) (PEG-10000) and absolute ethanol were produced by Tianjin Zhiyuan Chemical Reagent Co., Ltd. (Tianjin, China). N, N′-Methylene bis (acrylamide) (MBA) was purchased from Macklin Biochemical Co., Ltd. (Shanghai, China). 2-Hydroxy-4′-(2-Hydroxyethoxy)-2-Methylpropiophenone (Irgacure 2959, 98 %) was provided by Titan Scientific Co., Ltd. (Shanghai, China). Acrylamide (AM) was purchased from Sinopharm Chemical Reagent Co., Ltd.

2.2. Preparation of CNCs

CNCs were prepared by treating cotton (20 g) with H_2SO_4 solution (200 mL, 64 wt%) at 50 °C for 90 min under vigorous stirring. The solution was then diluted with deionized water (2 L) to terminate the reaction. After 24 h, the suspension was centrifuged at 10000 rpm for 5 min and washed with deionized water for 4 times until the solution didn't layer, dialyzed in deionized water with the dialysis bag (8000–14,000 kDa) for 5 days until the pH reached 6–7. Finally, the CNC suspension was concentrated to 3 wt% by rotary evaporator.

2.3. Preparation of CNCs-based and CNCs-g-PAM films

Irgacure 2959 and MBA were added to the AM aqueous solution (3 wt%), and the final mass ratio of AM/Irgacure 2959/MBA mass ratio was 100: 5: 5. The mixture was stirred for 1 h and ultrasonicated for 10 min under dark. The abovementioned polymerization systems were added to CNCs suspension (3 wt%) with vigorous stirring to reach the target CNCs/AM ratio of 8:2, 7:3, and 6:4. Then, 10 mL of mixture solution was poured into polystyrene Petri dishes (6 cm in diameter). EISA process was performed in a constant temperature and humidity chamber with relative humidity (RH) of 80 % at 25 °C in the dark. After one week of evaporation, the composite CNCs/AM films were obtained, which were further exposed to UV Lamp (395 nm, 300 W) for 120 s in a UV curing chamber (Gugou 2.0 UVFAST, China). The final hybrid CNCs-*g*-PAM films were denoted as CNCs-*g*-PAM-8:2, CNCs-*g*-PAM-7:3, and CNCs-*g*-PAM-6:4, respectively. The pure CNCs-based film was obtained without adding any other reagents under the same conditions. For other composite films, different polymers (i.e., PVA and PEG-10000) were added to CNCs suspension (3 wt%) with vigorous stirring to reach the target CNCs/polymer ratio of 8:2, and other operation conditions were the same as the preparation of CNCs-*g*-PAM films. The obtained composite films were marked as CNCs/PEG-10000 film and CNCs/PVA film, respectively.

2.4. Characterization

CNCs were first diluted to obtain CNCs suspension with a concentration of 0.01 wt% and further characterized by a transmission electron microscope (TEM) (JEM-F200, Japan) to get the particle morphology. The particle size and Zeta potential of the CNCs dispersion were measured by dynamic light scattering (DLS) using the Zeta sizer instrument (Malvern, Nano-ZS90, UK). The cross-section morphologies of CNCs-*g*-PAM films were observed by a scanning electron microscope (SEM) (S-8000, Hitachi, Japan) at an accelerating voltage of 5.0 kV after sprayed with a thin layer of gold. The chemical structure of the films was characterized by a Nicolet iN10 MX Fourier transform infrared (FT-IR) spectrometer (Thermo Scientific, USA), using the attenuated total reflection method in the range of 4000–400 cm^{-1} with a resolution of 4 cm^{-1}. The chiral nematic structure and birefringence of the CNCs-*g*-PAM films were proved by polarized optical microscopy (POM) (MX-117P, China). The crystal structure of the samples was recorded by an X-ray diffractometer (XRD) (Bruker D8, German) with Cu Kα radiation ranging from 5 to 80° at a rate of 2°/min and operated at a power of 40 kV with a current of 40 mA. The thermogravimetric analyzer (TGA) of all films was determined by a thermogravimetric analyzer (DTG-60, Shimadzu). UV–vis spectrophotometer (UV-2600, Shimadzu) was used to determine the UV–vis absorption spectra and transparency properties of all samples in the wavelength range of 200–800 nm. The wettability of the film surface was observed by the water contact angle (WCA, model SL200KB, SOLON TECH, Shanghai, China). A digital image was also taken during the contact angle measurements.

2.5. Mechanical property measurement

The samples were cut into a rectangular strip of 30 mm × 10 mm (length × width). The mechanical properties of films were measured by using the universal tensile testing machine (HD-B609B-S, China) at the stretching velocity of 0.5 mm·min^{-1}.

2.6. Swelling properties

The swelling properties were performed to study the solvent resistance of the as-prepared films. Also, the pure CNCs-based film, CNCs/PEG-10000 composite film, and CNCs/PVA composite film were used for comparison. In detail, the films were cut into rectangles (20 × 10 mm) and dried at 70 °C for 24 h to obtain the dry weights (W_d). Then, the dried films were immersed in the water at 25 °C for 24 h. The water on the surface of swollen films was adsorbed by the absorbent paper, and the wet weights (W_s) were recorded. The swelling ratio (SR) of the samples was calculated by the following formula.

$$SR(\%) = \frac{W_s}{W_d} \times 100 \quad (1)$$

3. Results and discussion

3.1. Characterizations of CNCs

The physicochemical properties of CNCs that significantly influenced the EISA process were characterized in this section. The as-prepared CNCs were typical rod-like shapes, and the average length and diameter were calculated to be 255 ± 15 nm and 34 ± 3 nm (Fig. S1), respectively. Also, the zeta potential of the CNCs was determined to explore the stability of the suspension system. Fig. S2 showed that the

zeta potential of as-prepared CNCs was −29.31 mV, and its absolute value was approximately 30 mV, indicating that the suspension could be facilely formed [22,23]. These results endowed the CNCs self-assembly.

3.2. Preparation and characterization of CNCs-g-PAM

Polyacrylamide is a well-known water-soluble polymer; due to its good water solubility and chemical activity, it is often used to prepare hydrogels and other materials [24,25]. The mechanism diagram of preparing CNCs-*g*-PAM hybrid films is shown in Fig. 1. In this study, CNCs-*g*-PAM was synthesized on the surface of CNCs by grafting acrylamide with Irgacure 2959 as a photo-initiator. This reaction can occur in an aqueous solution, and acrylamide can be grafted onto surfaces of various materials [26]. Irgacure 2959 formed a redox system with the hydroxyl group on the surface of CNCs to generate macromolecular radicals. This led to the graft polymerization of acrylamide on CNCs to produce CNCs-*g*-PAM film.

To certify the chemical structures of the CNCs-*g*-PAM films, FT-IR measurement was performed on the neat CNCs-based and CNCs-*g*-PAM films. FT-IR results of the obtained films are used to analyze the chemical variation among CNCs-based film, PAM, and CNCs-*g*-PAM films (Fig. 2A). For CNCs-based and CNCs-*g*-PAM films, the characteristic peaks at 2900 cm^{-1}, 1365 cm^{-1} and 668 cm^{-1} were ascribed to the C-H stretching, C-H deformation vibration, and C-OH out-of-plane bending mode, respectively [27]. C-O-C, C-C-O, and C-C-H deformation modes and stretching vibrations of the C-5 and C-6 atoms located at 900 cm^{-1} [28]. The peak at 1110 and 1056 cm^{-1} came from -CH_2-O-CH_2 stretching vibration of the pyranose ring and β-glycosidic bond of the CNCs in CNCs-*g*-PAM. Moreover, the stretching vibration of the hydroxyl groups could be found in the range of 3660–2998 cm^{-1}. The stretching vibration of primary amide was located at 3329 cm^{-1} and 3164 cm^{-1}. The stretching vibration of -NH_2 groups gradually emerged with the increasing dosage of AM in the spectra of CNCs-*g*-PAM films. For the CNCs-*g*-PAM films, the generated peaks at 1656 cm^{-1} (C=O) and 1602 cm^{-1} (N—H) were assigned to the characteristic absorption bands of amide-I and amide-II of PAM [29]. These results indicated that PAM was successfully grafted onto the CNCs.

The crystalline structure of the CNCs-based and CNCs-*g*-PAM films was recorded by X-ray diffraction (XRD) analysis from Fig. 2B. The characteristic diffraction peaks of CNCs were located at 14.78°, 16.43°, 22.61°, and 34.43°, corresponding to the (1 $\bar{1}$ 0), (110), (200), and (004) planes of cellulose I_β [30,31]. In terms of the CNCs-*g*-PAM, the CNCs-*g*-PAM films also showed the same peaks, which demonstrated that the graft polymerization did not change the crystal structure. However, the crystallinity of the obtained films was calculated using MDI JADE 6.5, and the crystallinities of CNCs, CNCs-*g*-PAM-8:2, CNCs-*g*-PAM-7:3, and CNCs-*g*-PAM-6:4 films were 78.14 %, 74.34 %, 71.22 %, and 67.14 %, respectively. These results showed that the dosage of PAM contributed to disrupting the ordered structure of CNCs, i.e., the amide groups could weaken the intermolecular hydrogen bond among cellulose units and consequently destroy the crystalline structure of cellulose. Although the hydroxyl groups have a higher ability to form hydrogen bondings than the amino groups, the amino group will form a competitive relationship with the hydroxyl group that has formed hydrogen bonding when the amino group is present, which may cause the destruction of the crystalline structure of the surface layer of CNCs.

Fig. 2C shows the thermo stability of the as-prepared films, including the CNCs-based film and CNCs-*g*-PAM films. The pyrolysis process of pure CNCs-based film can be divided into three stages. The initial decomposition temperature was around 130 °C, attributed to the evaporation of free moisture and adsorbed water in the film [32]. The second stage in the temperature range of 138– 270 °C was due to the catalytic dehydration on the surface of CNCs by sulfate hemiester groups, and the DTG curves (Fig. 2D) showed two separated pyrolysis peaks [33,34], which was similar to the published data. The peak temperatures of CNCs were 188 °C and 270 °C, and their weight loss ratio was 23.23 % and 20.86 %, respectively. The final stage that occurred at 330– 500 °C was the slow carbonization of solid residue, viz., the biochar was obtained. The TG curves of CNCs-*g*-PAM films indicated that the decomposition temperature was higher than 240 °C, much higher than the initial decomposition temperature of CNCs (188 °C). This enhanced phenomenon may be due to the surface coating of PAM on CNCs that significantly blocked the heat transfer. Also, the amide can act as a proton acceptor that decreases the proton-catalyzed hydrolysis.

3.3. SEM analysis

The micromorphology of native CNCs-based film and CNCs-*g*-PAM hybrid films was observed by SEM. As shown in Fig. 3A, the pure CNCs-based film retained a layered structure with a constant distance, specifically manifested as the excellent self-assembly properties within the solid film. This structural image revealed the left-handed spiral orientation and highly ordered chiral nematic structure [35]. The SEM images of CNCs-*g*-PAM films are shown in Figs. 3 B—D, from which we can find a structure similar to that of pure CNCs-based film, confirming the structural integrity of the CNCs-*g*-PAM films. Similar observations were previously reported by Tao et al. [29].

The cross-linking of CNCs with PAM might change the chiral nematic pitch of the films. The distance between adjacent layers represented half of the helical distance of the chiral nematic structure. The pitch values calculated from the SEM images were 0.51, 0.57, 0.60, and 0.68 μm for CNCs-based, CNCs-*g*-PAM-8:2, CNCs-*g*-PAM-7:3, and CNCs-*g*-PAM-6:4

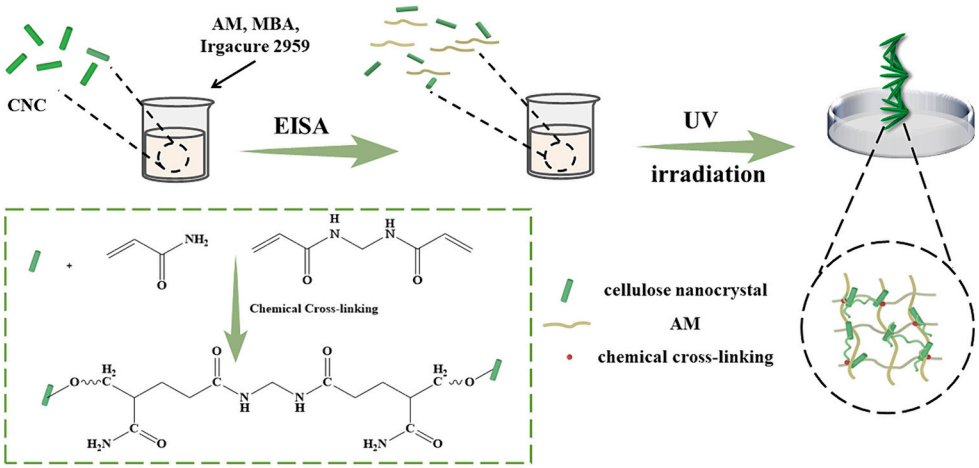

Fig. 1. Schematic illustration of the fabrication process and network microscopic structure of CNCs-*g*-PAM films.

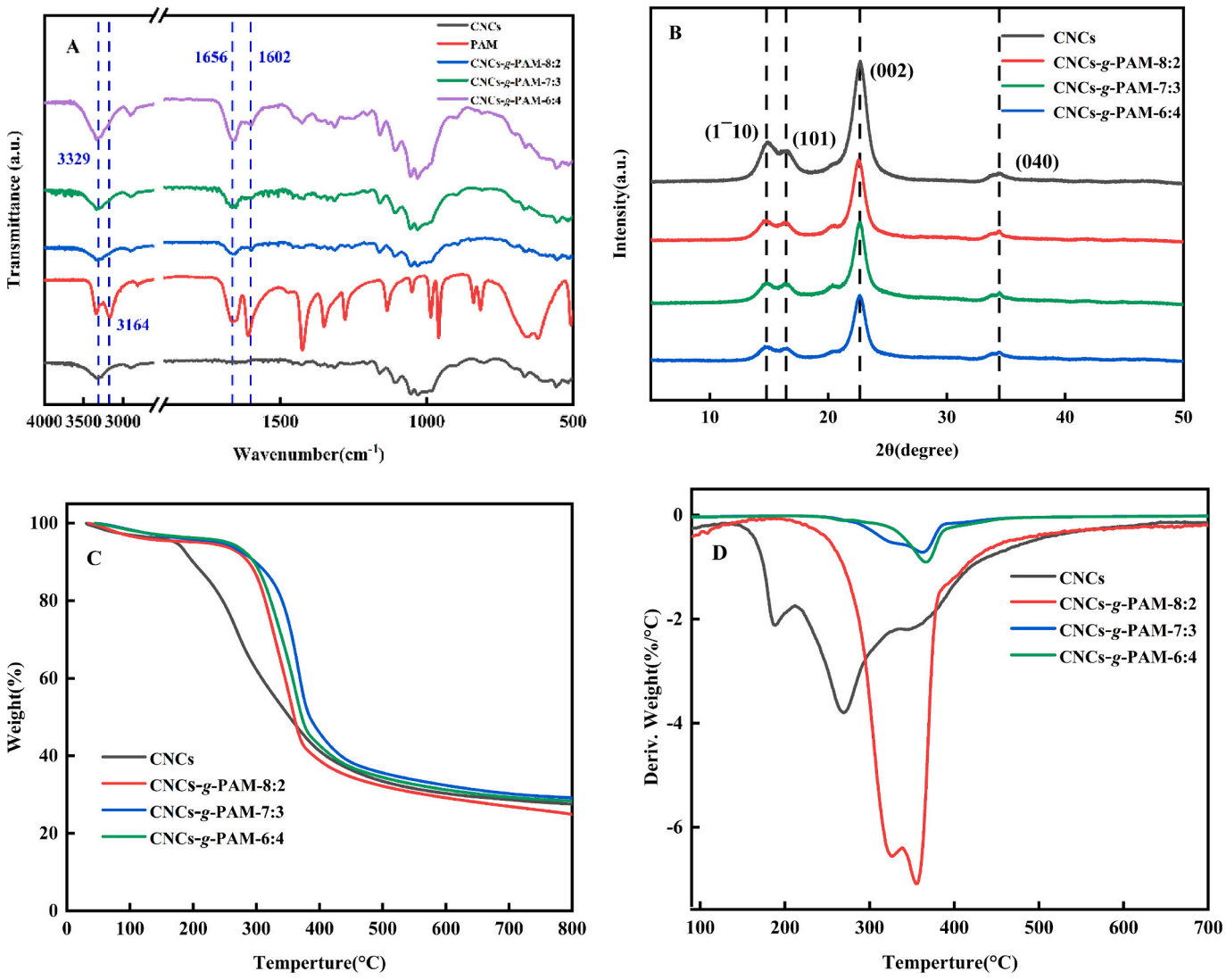

Fig. 2. Chemical characterizations of CNCs-*g*-PAM films. (A) The FT-IR spectra of CNCs-based film, PAM, and CNCs-*g*-PAM films; (B) The XRD patterns of CNCs-based and CNCs-*g*-PAM films; (C) The thermo-stability of the CNCs and CNCs-*g*-PAM films; (D) The DTG curves of the as-prepared films.

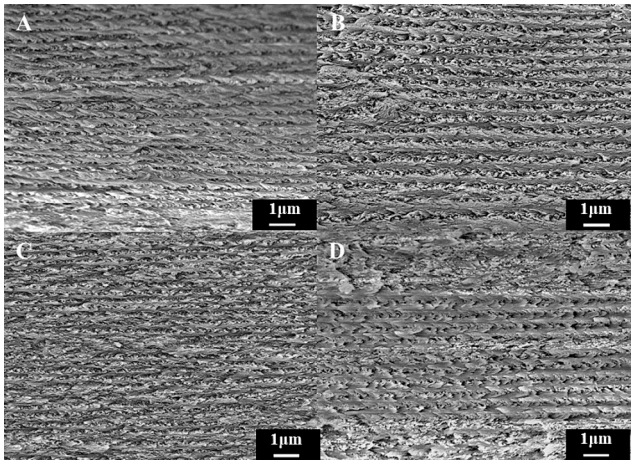

Fig. 3. The SEM images (10,000 ×) on the cross-section of (A) native CNCs-based film, (B) CNCs-*g*-PAM-8:2, (C) CNCs-*g*-PAM-7:3, and (D) CNCs-*g*-PAM-6:4 films.

films, respectively. This increasing trend may be induced by the surface coating of PAM on CNCs. These results also indicated that the surface polymerization strategy could be used to adjust the chiral nematic pitch of CNCs-based chiral nematic film.

The helicoidal ordering retained in the dried films resulted in interesting optical properties. The film can selectively reflect light with wavelengths that depend on the pitch length. According to Bragg's law [36], $\lambda_{max} = n_{avg} P \sin\theta$, where n_{avg}, P, θ represented the average refractive index, the helical pitch length, and the angle between the incident light and the cholesteric layers, respectively. As CNCs and PAM have similar refractive indices of 1.55 and 1.46 [35,37], the differences in n_{avg} among the films with different CNCs-*g*-PAM ratios were almost negligible [38]. Therefore, the helical pitch was similar to the wavelength of the visible light between 400 and 700 nm, and the pitch of the obtained films was in the visible range, which can show structural colors [39].

3.4. The macrograph and POM of CNCs and CNCs-g-PAM films

The photographs of the prepared hybrid film are shown in Fig. 4A; the surface of the film was flat and transparent without any deformation or cracking. The color of the obtained films was macroscopically uniform and presented a light blue. To investigate the effect of AM on the

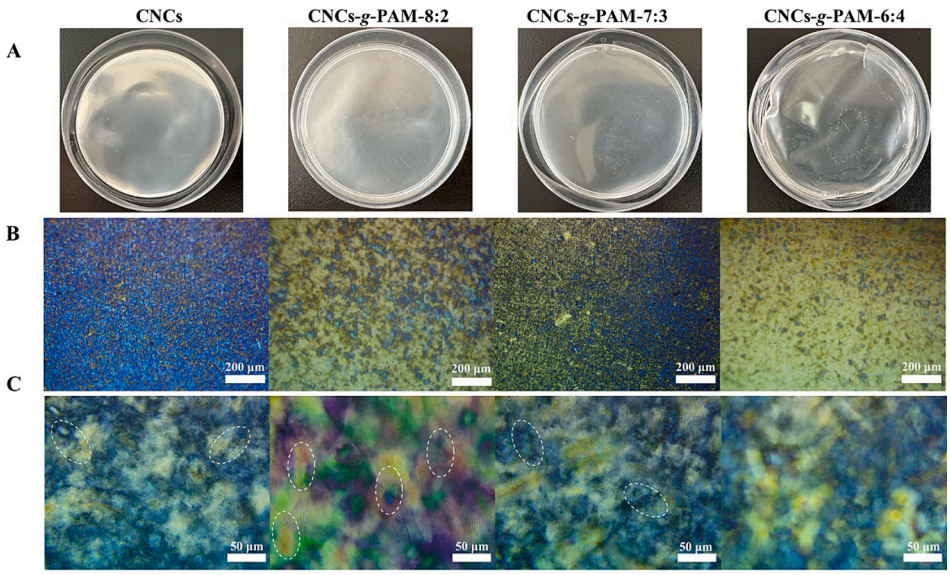

Fig. 4. Photographs (A) (1 cm) and POM images (B, C) (scale bar, 200 and 50 μm) of the CNCs-based and CNCs-*g*-PAM films. The micrograph was taken with a crossed polarizer.

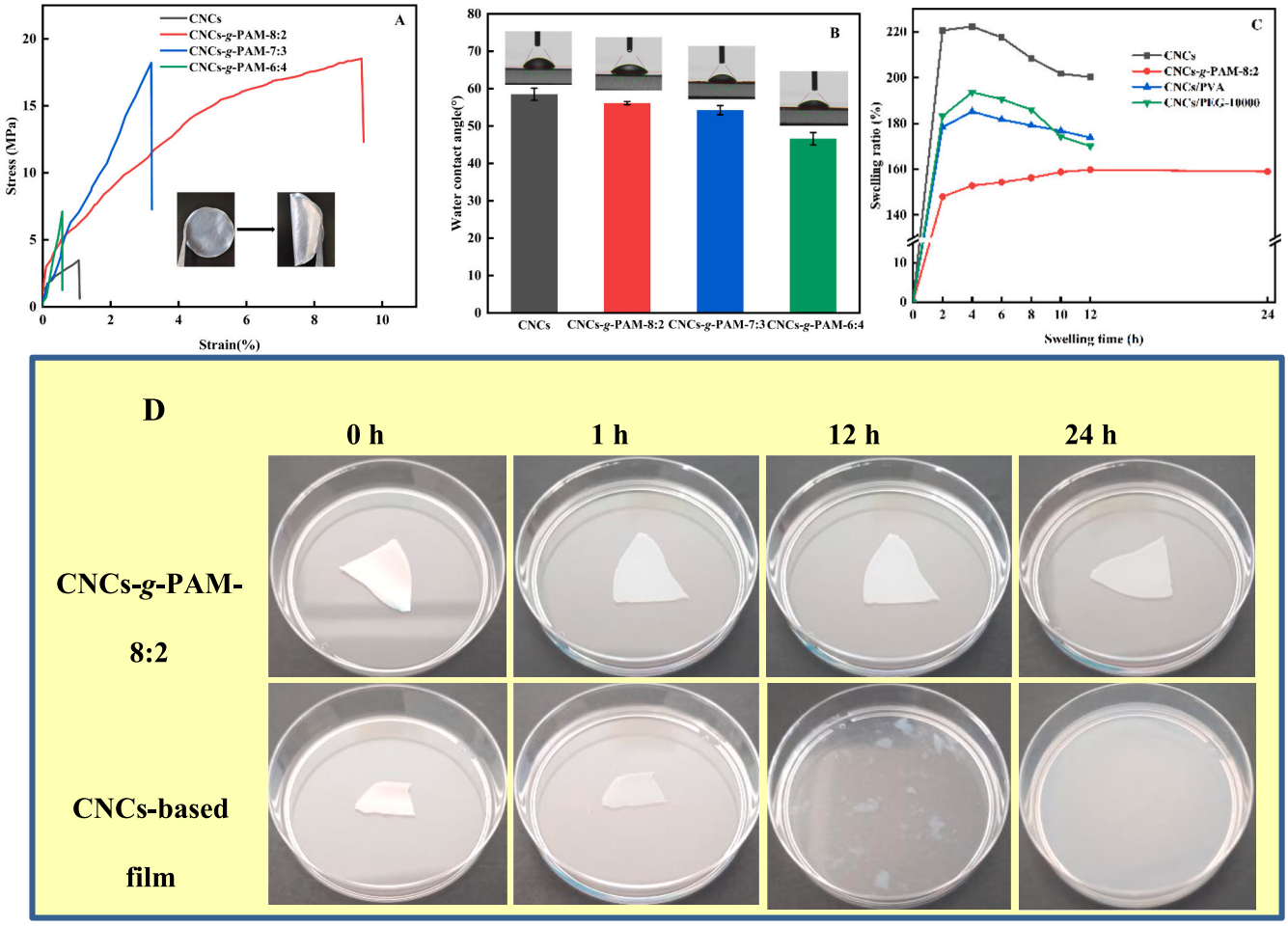

Fig. 5. (A) The stress-strain curves of CNCs and CNCs-*g*-PAM films, and the inset was a bending picture of CNCs-*g*-PAM-8:2 film. (B) Contact angles of the CNCs and CNCs-*g*-PAM films. (C) The swelling properties of different CNCs-containing films (i.e., CNCs, CNCs-*g*-PAM film-8:2, CNCs/PVA, and CNCs/PEG-10000 films); (D) Pictures of the CNCs-based film and CNCs-*g*-PAM-8:2 that immersed in water for different times, from which we can found the tolerance to water of the films that prepared from different preparation process (chemical crosslinking and physical self-assembly) and feedstocks (CNCs-PAM and pure CNCs).

chiral nematic structure of CNCs, we used polarized optical microscopy (POM) to verified the structure of the films, as shown in Figs. 4 B—C. It could be seen that the pure CNCs-based film and CNCs-*g*-PAM films had apparent cholesteric liquid crystal structure and finger texture, as long as PAM content was less than 30 %. However, the CNCs-*g*-PAM-6:4 film had some degree of crimp and cracking from a macroscopical view. In addition, the fingerprint region vanished and did not show birefringence like the other samples under a 40-fold polarizing microscope, which might originate from the phase separation in the film, hindering the self-assembly of CNCs [40]. The obtained film became transparent, suggesting that no chiral nematic structure was acquired at this volume ratio.

3.5. Mechanical properties of the as-prepared films

Mechanical properties were one of the most important indexes for a film material, regardless of which application it was used in. Here, we evaluated and compared the mechanical properties of pure CNCs composite film and CNCs-*g*-PAM hybrid films. The CNCs-based film showed a tensile strength of 3.5 MPa and the elongation at break of 1.1 % (Fig. 5A), indicating the fragility of CNCs-based film via the EISA process. Generally, the ordinary CNCs-*g*-PAM hybrid films showed much better mechanical properties than the CNCs-based film via the EISA process in both tensile strength and elongation at break. Fig. 5A also manifested these performances of the as-prepared CNCs-*g*-PAM films via the combination of free radical polymerization and EISA strategies. It was clear that the tensile strength and the elongation at break were all improved via this synergy strategy. Thereinto, the CNCs-*g*-PAM-8:2 film expressed the best performances, viz., the tensile strength achieved 18.5 MPa, and the elongation at break was 9.4 %, which was 5.3 times and 8.5 times of the CNCs-based composite film via the EISA process, respectively. As shown in the inset, the CNCs-*g*-PAM-8:2 film can be easily bent, presenting good flexibility that can hardly be realized for the pure CNCs-based film. This phenomenon was undoubtedly induced by the covalent crosslinking. Moreover, hydrogen bonding and electrostatic interaction may also play an essential role in this process.

3.6. Wettability and swelling behavior of the as-prepared films

For a film material, the application can not avoid the contact to moisture in the atmosphere. Thus, the wettability and the swelling behavior are also significant. However, the published data generally focused on forming the CNCs-based composite films (e.g., pure CNCs-based film, CNCs/PEG-10000 film, and CNCs/PVA film) via EISA, which would undoubtedly be dissolved in the aqueous solution due to the great hydrophilia of the feedstocks. Here, we determined the wettability and swelling behavior of the as-prepared covalent films and compared them with the CNCs-based composite films.

Fig. 5B showed that the water contact angles (WCA) of all the photonic crystal films were below 90°, indicating the hydrophilia of the as-prepared films induced by excellent hydrophilia of CNCs and PAM. This hydrophilia contributed to the biocompatibility of the as-prepared film that can be ultimately degraded by microflora. So, this work confirms the high importance of CNCs and the other bioactive compounds in different fields. Moreover, the WCA values of CNCs-*g*-PAM films were smaller than that of pure CNCs-based film, and they decreased with the increasing dosage of PAM. This phenomenon may be induced by the high hydrophilicity of PAM [47].

Swelling behavior was the joint appearance for a hydrophilic film or matrix. These properties of the as-prepared films were determined, shown in Fig. 5C. The films all exhibited quick water adsorption in the first 2 h and reached their extremes in 4 h. Moreover, the composite films decreased the swelling ratios, presenting the degradation of the as-prepared composite films, including the pure CNCs-based film, CNCs/PEG-10000 film, and CNCs/PVA film. The CNCs-*g*-PAM-8:2 film showed the lowest swelling ratio among the four films due to the strong covalent forces. The pictures of the CNCs-based film and CNCs-*g*-PAM-8:2 immersed in water are shown in Fig. 5D. We can find that the CNCs-based film gradually dissolved in the water, indicating the instability toward water and meaningless for many applications. The color of CNCs-based film and CNCs-*g*-PAM-8:2 clearly changed after immersing in water due to the change in screw pitch. The CNCs-*g*-PAM-8:2 was also immersed in alcohol, and the apparent color was different from that in water (Fig. S3). This phenomenon may be induced by the different affinity between CNCs-*g*-PAM-8:2 and the solvents (i.e., water and alcohol).

3.7. Optical properties of the films

The UV–Vis transmittance of the CNCs and CNCs-*g*-PAM films was measured within the 200– 800 nm wavelength range. All films represented high transparency with transmittance at 550 nm above 75 % (Fig. 6A). This results are different from the cellulose-based flims that also have a super high transparency in the visible light region (400–700 nm) [48,49]. Kurihara and Isogai prepared TEMPO-oxidized cellulose nanofibril/PAM composite film and found that the light transmittance was close to 100 % when the wavelengths were higher than 350 nm [49]. This phenomenon was due to formed anisotropic arrangement that can selectively reflect circularly polarized light [29,50]. Moreover, the performance of filtering UV light can be used in the field of light management that helps to reduce diseases caused by too much UV exposure, consequently benefiting human health [52]. The maximum transmittance of the CNCs and different CNCs-*g*-PAM films at approximately 800 nm was 89.3 %, 90.4 %, 88.7 %, and 94.8 %, respectively. To present the transparency of the CNCs-*g*-PAM-8:2 film more intuitively, the light transparency was visualized by putting this over a pattern (insert in Fig. 6A). The background pattern was clearly seen, indicating that the films were highly transparent and indistinguishable from each other under daylight. However, the films we prepared have a low transmittance (30 %) in the ultraviolet region (200– 400 nm). This may be because the structure of CNCs is absorbed, similar to the previous report [53]. Moreover, through the absorption curve of the films, CNCs and CNCs-*g*-PAM films have the same absorption peaks in the absorption curve of the UV region, as shown in Fig. 6B. It was caused by the chiral nematic liquid crystal structure of CNCs, especially for the ultraviolet band [54].

4. Conclusion

In summary, we fabricated a novel CNCs-based photonic crystal films with high toughness by the combination of free radical polymerization and EISA strategies. The water-soluble PAM was covalently bonded to CNCs. The variation of the PAM content did not alter the chiral nematic structure but the screw pitch of the films. Due to covalent bonding, the CNCs-*g*-PAM film had good thermostability and mechanical properties with an elongation at break of about 9 % and a tensile strength of 18.5 MPa. The wettability of the as-prepared films decreased with the increasing content of PAM; however, the swelling ratio of the CNCs-*g*-PAM-8:2 was smaller than that of other CNCs-based composite films (i.e., CNCs/PVA and CNCs/PEG-10000 composite films) and showed resistance to water for more than 24 h. Based on the above properties, the CNCs-*g*-PAM films could be expected to show applications in light management, anti-counterfeiting, and decorative coatings.

CRediT authorship contribution statement

Yue Zhang: Writing – original draft, Visualization, Validation, Resources, Methodology, Investigation, Data curation, Conceptualization. **De-qiang Li:** Writing – original draft, Visualization, Validation, Supervision, Resources, Methodology, Funding acquisition, Formal analysis. **Cai-xia Yang:** Writing – original draft, Resources, Methodology. **Zi-wei Xiong:** Methodology, Investigation, Data curation. **Maryamgul Tohti:**

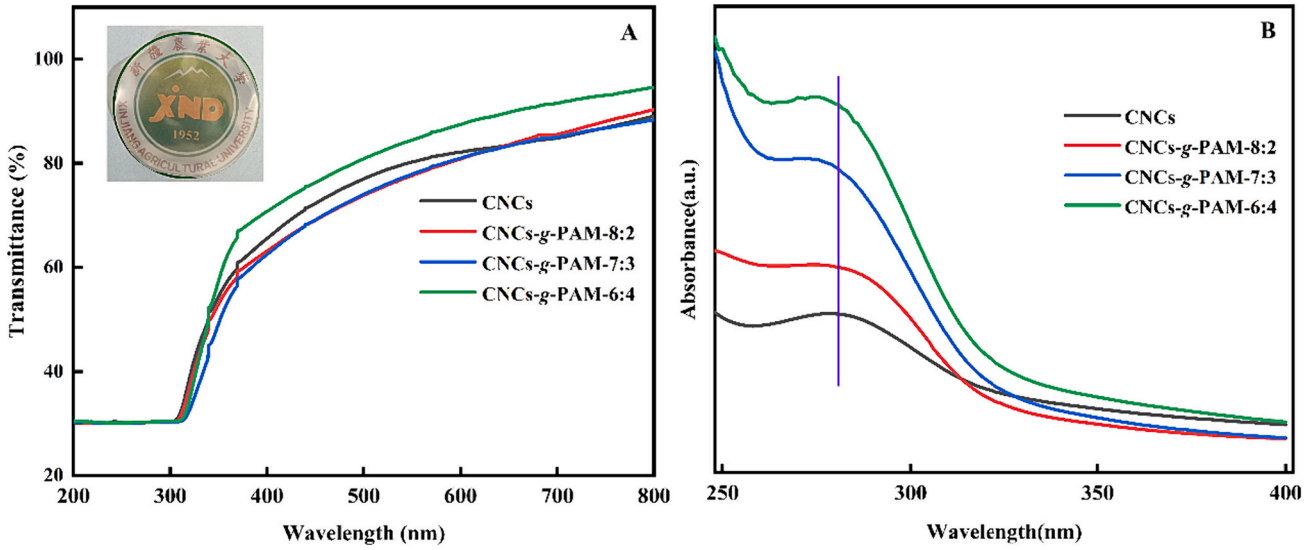

Fig. 6. (A) The UV–vis transmittance (the inset showing the CNCs-*g*-PAM-8:2 film placed on an "emblem" pattern) and (B) UV–vis spectra of the CNCs and CNCs-*g*-PAM films.

Writing – original draft, Investigation, Data curation. **Yu-qing Zhang:** Visualization, Validation, Resources. **Hong-jie Chen:** Investigation. **Jun Li:** Writing – original draft, Visualization, Validation, Resources, Methodology, Funding acquisition, Formal analysis.

Declaration of competing interest

The authors declare that they have no competing financial interests.

Data availability

Data will be made available on request.

Acknowledgment

The present work was supported by the Natural Science Foundation of Xinjiang (No. 2021D01A74), the Project of Tianshan Innovation Team Plan of Xinjiang, China (No. 2023D14020), and the Tianshan Talent Training Program of Xinjiang, China (2023TSYCCX0039).

Appendix A. Supplementary data

Supplementary data to this article can be found online at https://doi.org/10.1016/j.ijbiomac.2024.130793.

References

[1] M. Giese, M. Spengler, Cellulose nanocrystals in Nanoarchitectonics – towards photonic functional materials, Mol. Syst. Des. Eng. 4 (2019) 29–48, https://doi.org/10.1039/C8ME00065D.
[2] X. Yang, X. Jin, T. Zhao, P. Duan, Circularly polarized luminescence in chiral nematic liquid crystals: generation and amplification, Mater. Chem. Front. 5 (2021) 4821–4832, https://doi.org/10.1039/D1QM00335F.
[3] A. Gowda, S.K. Pathak, G.A.R. Rohaley, G. Acharjee, A. Oprandi, R. Williams, M. E. Prévôt, T. Hegmann, Organic chiral nano- and microfilaments: types, formation, and template applications, Mater. Horiz. 11 (2024) 316–340, https://doi.org/10.1039/D3MH01390A.
[4] X. Zou, R. Xue, Z. An, H. Li, J. Zhang, Y. Jiang, L. Huang, W. Wu, S. Wang, G.H. Hu, R.K.Y. Li, H. Zhao, Recent advances in flexible CNC-based chiral nematic film materials, Small 20 (2024) 2303778, https://doi.org/10.1002/smll.202303778.
[5] H. Chanzy, A. Peguy, S. Chaunis, P. Monzie, Oriented cellulose films and fibers from a mesophase system, J. Polym. Sci. Polym. Phys. Ed. 18 (1980) 1137–1144, https://doi.org/10.1002/pol.1980.180180517.
[6] T. Odijk, H.N.W. Lekkerkerker, Theory of the isotropic-liquid crystal phase separation for a solution of bidisperse rodlike macromolecules, J. Phys. Chem. C. 89 (1985) 380–381.
[7] A. Stroobants, H.N.W. Lekkerkerker, T. Odijk, Effect of electrostatic interaction on the liquid crystal phase transition in solutions of rodlike polyelectrolytes, Macromolecules 19 (1986) 2232–2238, https://doi.org/10.1021/ma00162a020.
[8] U. Casado, V.L. Mucci, M.I. Aranguren, Cellulose nanocrystals suspensions: liquid crystal anisotropy, rheology and films iridescence, Carbohydr. Polym. 261 (2021) 117848, https://doi.org/10.1016/j.carbpol.2021.117848.
[9] J.P. Ge, Y.D. Yin, Responsive photonic crystals, Angew. Chem. Int. Ed. 50 (2011) 1492–1522, https://doi.org/10.1002/anie.200907091.
[10] D. Nepal, S. Kang, K.M. Adstedt, K. Kanhaiya, M.R. Bockstaller, L.C. Brinson, M. J. Buehler, P.V. Coveney, K. Dayal, J.A. El-Awady, L.C. Henderson, D.L. Kaplan, S. Keten, N.A. Kotov, G.C. Schatz, S. Vignolini, F. Vollrath, Y. Wang, B.I. Yakobson, V.V. Tsukruk, H. Heinz, Hierarchically structured bioinspired nanocomposites, Nat. Mater. 22 (2022) 18–35, https://doi.org/10.1038/s41563-022-01384-1.
[11] C. Chen, W. Sun, J. Wang, D.J. Gardner, Tunable biocomposite films fabricated using cellulose nanocrystals and additives for food packaging, Carbohydr. Polym. 321 (2023) 121315, https://doi.org/10.1016/j.carbpol.2023.121315.
[12] F. Su, D. Liu, M. Li, Q. Li, Ch. Liu, L. Liu, J. He, H. Qiao, Mesophase transition of cellulose nanocrystals aroused by the incorporation of two cellulose derivatives, Carbohydr. Polym. 233 (2020) 115843, https://doi.org/10.1016/j.carbpol.2020.115843.
[13] V. Vatanpour, O.O. Teber, M. Mehrabi, I. Koyuncu, Polyvinyl alcohol-based separation membranes: a comprehensive review on fabrication techniques, applications and future prospective, Mater. Today Chem. 28 (2023) 101381, https://doi.org/10.1016/j.mtchem.2023.101381.
[14] H.S. Park, S.-W. Kang, L Tortora, S. Kumar, O.D. Lavrentovich, Condensation of self-assembled lyotropic chromonic liquid crystal sunset yellow in aqueous solutions crowded with polyethylene glycol and doped with salt, Langmuir 27 (7) (2011) 4164–4175, https://doi.org/10.1021/la200505y.
[15] M.Q. Lin, V.S. Raghuwanshi, C. Browne, G.P. Simon, G. Garnier, Modulating transparency and colour of cellulose nanocrystal composite films by varying polymer molecular weight, J. Colloid Interface Sci. 584 (2021) 216–224, https://doi.org/10.1016/j.jcis.2020.09.123.
[16] M. Liu, K. Kuang, G. Li, Sh. Yang, Z. Yuan, Photoluminescence-enhanced cholesteric films: Coassembling copper nanoclusters with cellulose nanocrystals, Carbohydr. Polym. 257 (2021) 117641, https://doi.org/10.1016/j.carbpol.2021.117641.
[17] M.A. Javaid, S. Jabeen, N. Arshad, K.M. Zia, M.T. Hussain, I. Ullah, S. Ahmad, M. Shoaib, Preparation of amylopectin and chitosan based polyurethanes for sustained drug release studies, Sustain. Chem. Pharm. 33 (2023) 101086, https://doi.org/10.1016/j.scp.2023.101086.
[18] N. Arshad, M.A. Javaid, K.M. Zia, M.T. Hussain, M.M. Arshad, U. Tahir, Development of biocompatible aqueous polyurethane dispersions using chitosan and curcumin to improve physicochemical properties of textile surfaces, Int. J. Biol. Macromol. 251 (2023) 126196, https://doi.org/10.1016/j.ijbiomac.2023.126196.
[19] M.A. Javaid, S. Jabeen, N. Arshad, K.M. Zia, M.T. Hussain, I.A. Bhatti, A. Iqbal, S. Ahmad, I. Ullah, Development of amylopectin based polyurethanes for sustained drug release studies, Int. J. Biol. Macromol. 244 (2023) 125224, https://doi.org/10.1016/j.ijbiomac.2023.125224.
[20] A. Etale, A.J. Onyianta, S.R. Turner, S.J. Eichhorn, Cellulose: a review of water interactions, applications in composites, and water treatment, Chem. Rev. 123 (2023) 2016–2048, https://doi.org/10.1021/acs.chemrev.2c00477.
[21] C. Gomri, M. Cretin, Recent progress on chemical modification of cellulose nanocrystal (CNC) and its application in nanocomposite films and membranes-a

comprehensive review, Carbohydr. Polym. 294 (2022) 119790, https://doi.org/10.1016/j.carbpol.2022.119790.
[22] H. Mirhosseini, C.P. Tan, N.S.A. Hamid, S. Yusof, Effect of Arabic gum, xanthan gum and orange oil contents on ζ-potential, conductivity, stability, size index and pH of orange beverage emulsion, Colloid. Surface A 315 (2008) 47–56, https://doi.org/10.1016/j.colsurfa.2007.07.007.
[23] C.X. Yang, J. Li, Y.Q. Zhang, Ch. Wu, D.Q. Li, A pesticide sustained-release microcapsule from cellulose nanocrystal stabilized Pickering emulsion template, J. Appl. Polym. Sci. 140 (2023) e53716, https://doi.org/10.1002/app.53716.
[24] B. Li, Y. Zhang, Ch. Wu, B. Guo, Zh. Luo, Fabrication of mechanically tough and self-recoverable nanocomposite hydrogels from polyacrylamide grafted cellulose nanocrystal and poly(acrylic acid), Carbohydr. Polym. 198 (2018) 1–8, https://doi.org/10.1016/j.carbpol.2018.06.047.
[25] J.A. Kelly, A.M. Shukaliak, C.C. Cheung, K.E. Shopsowitz, W.Y. Hamad, M. J. MacLachlan, Responsive photonic hydrogels based on nanocrystalline cellulose, Angew. Chem. Int. Ed. 52 (2013) 8912–8916, https://doi.org/10.1002/anie.201302687.
[26] Y. Habibi, Key advances in the chemical modification of nanocelluloses, Chem. Soc. Rev. 43 (2014) 1519–1542, https://doi.org/10.1039/c3cs60204d.
[27] L.M. Proniewicz, C. Paluszkiewicz, A. Wesełucha-Birczyńska, H. Majcherczyk, A. Barański, A. Konieczna, FT-IR and FT-Raman study of hydrothermally degradated cellulose, J. Mol. Struct. 596 (2001) 163–169, https://doi.org/10.1016/S0022-2860(01)00706-2.
[28] S.Y. Oh, D.I. Yoo, Y. Shin, G. Seo, FTIR analysis of cellulose treated with sodium hydroxide and carbon dioxide, Carbohydr. Res. 340 (2005) 417–428, https://doi.org/10.1016/j.carres.2004.11.027.
[29] T. Lu, H. Pan, J. Ma, Y. Li, S.W. Bokhari, X.L. Jiang, S.M. Zhu, D. Zhang, Cellulose nanocrystals/polyacrylamide composites of high sensitivity and cycling performance to gauge humidity, ACS Appl. Mater. Interfaces. 9 (21) (2017) 18231–18237, https://doi.org/10.1021/acsami.7b04590.
[30] N. Lin, A. Dufresne, Surface chemistry, morphological analysis and properties of cellulose nanocrystals with gradiented sulfation degrees, Nanoscale 6 (2014) 5384–5393, https://doi.org/10.1039/c3nr06761k.
[31] S. Eyley, W. Thielemans, Surface modification of cellulose nanocrystals, Nanoscale 6 (2014) 7764–7779, https://doi.org/10.1039/c4nr01756k.
[32] Y.-q. Zhang, J. Li, X.-j. Huang, C.-x. Yang, Ch. Wu, Z.-l. Yang, D.-Q. Li, Performance-enhanced regenerated cellulose film by adding grape seed extract, Int. J. Biol. Macromol. 232 (2023) 123290, https://doi.org/10.1016/j.ijbiomac.2023.123290.
[33] N. Wang, E. Ding, R. Cheng, Thermal degradation behaviors of spherical cellulose nanocrystals with sulfate groups, Polymer 48 (2007) 3486–3493, https://doi.org/10.1016/j.polymer.2007.03.062.
[34] M. Roman, W.T. Winter, Effect of sulfate groups from sulfuric acid hydrolysis on the thermal degradation behavior of bacterial cellulose, Biomacromolecules 5 (2004) 1671–1677.
[35] A.G. Dumanli, H.M. van der Kooij, G. Kamita, E. Reisner, J.J. Baumberg, U. Steiner, S. Vignolini, Digital color in cellulose nanocrystal films, ACS Appl. Mater. Interfaces 6 (2014) 12302–12306, https://doi.org/10.1021/am501995e.
[36] R.R. da Rosa, P.E.S. Silva, D.V. Saraiva, A. Kumar, A.P.M. de Sousa, P. Sebastião, S. N. Fernandes, M.H. Godinho, Cellulose nanocrystal aqueous colloidal suspensions: evidence of density inversion at the isotropic-liquid crystal phase transition, Adv. Mater. 34 (2022) 2108227, https://doi.org/10.1002/adma.202108227.
[37] E. Lizundia, D. Puglia, T.-D. Nguyen, I. Armentano, Cellulose nanocrystal based multifunctional nanohybrids, Prog. Mater. Sci. 112 (2020) 100668, https://doi.org/10.1016/j.pmatsci.2020.100668.
[38] Y. Huang, G. Chen, Q. Liang, Z. Yang, H. Shen, Multifunctional cellulose nanocrystal structural colored film with good flexibility and water-resistance, Int. J. Biol. Macromol. 149 (2020) 819–825, https://doi.org/10.1016/j.ijbiomac.2020.01.247.
[39] K.F. Wissbrun, Rheology of Rodlike polymers in the liquid crystalline state, J. Rheol. 25 (1981) 619–662, https://doi.org/10.1122/1.549634.
[40] Y. Sui, X. Li, W. Chang, H. Wan, W. Li, F. Yang, Z.Z. Yu, Multi-responsive nanocomposite membranes of cellulose nanocrystals and poly(N-isopropyl acrylamide) with tunable chiral nematic structures, Carbohydr. Polym. 232 (2020) 115778, https://doi.org/10.1016/j.carbpol.2019.115778.
[47] S. Wu, R.A. Shanks, Solubility study of polyacrylamide in polar solvents, J. Appl. Polym. Sci. 93 (2004) 1493–1499, https://doi.org/10.1002/app.20608.
[48] B.-X. Zhang, J.-I. Azuma, H. Uyama, Preparation and characterization of a transparent amorphous cellulose film, RSC Adv. 5 (2015) 2900–2907, https://doi.org/10.1039/C4RA14090G.
[49] T. Kurihara, A. Isogai, Properties of poly(acrylamide)/TEMPO-oxidized cellulose nanofibril composite films, Cellulose 21 (2014) 291–299, https://doi.org/10.1007/s10570-013-0124-z.
[50] C. Verma, M. Chhajed, S. Singh, P.K. Maji, Cellulose nanocrystals for environment-friendly self-assembled stimuli doped multisensing photonics, ACS Appl. Polym. Mater. 4 (2022) 4047–4068, https://doi.org/10.1021/acsapm.2c00061.
[52] Y. Song, Y. Xu, D. Li, S. Chen, F. Xu, Sustainable and Superhydrophobic lignocellulose-based transparent films with efficient light management and self-cleaning, ACS Appl. Mater. Interfaces 13 (2021) 49340–49347, https://doi.org/10.1021/acsami.1c14948.
[53] F. Huang, X. Wu, Y. Yu, Y. Lu, Q. Chen, Acylation of cellulose nanocrystals with acids/trifluoroacetic anhydride and properties of films from esters of CNCs, Carbohydr. Polym. 155 (2017) 525–534, https://doi.org/10.1016/j.carbpol.2016.09.010.
[54] T.G. Parton, R.M. Parker, G.T. van de Kerkhof, A. Narkevicius, J.S. Haataja, B. Frka-Petesic, S. Vignolini, Chiral self-assembly of cellulose nanocrystals is driven by crystallite bundles, Nat. Commun. 13 (2022) 2657, https://doi.org/10.1038/s41467-022-30226-6.